Charalampous, A., Yuan, X., McNeill, N., Walder, S., Yan, Q., & Frederickson, C. (2016). Controlling the output voltage frequency response of the auxiliary commutated pole inverter. In 42nd Annual Conference of the IEEE Industrial Electronics Society, IECON 2016. (pp. 3305-3310). Institute of Electrical and Electronics Engineers (IEEE). DOI: 10.1109/IECON.2016.7793828

Controlling the Output Voltage Frequency Response of the Auxiliary Commutated Pole Inverter

Apollo Charalambous, Xibo Yuan, Neville McNeill, Sam Walder, Qingzeng Yan, and Clive Frederickson
Department of Electrical & Electronic Engineering
University of Bristol
Bristol, United Kingdom
apollo.charalambous@bristol.ac.uk

***Abstract*—The auxiliary commutated pole inverter (ACPI) is a PWM soft-switching topology usually employed for switching loss reduction. This work however investigates how the two traditional ACPI control schemes, fixed- and variable-timing, can shape the transitioning edges of the inverter's output voltage. Its frequency response can then be predicted and its high-frequency content mitigated, with potential enhancements to the inverter's Common Mode Electromagnetic Interference (CM EMI) performance. By addressing the EMI problem at source, lighter passive filters might be used, beneficial to applications where high power densities are desirable. A 5-kW, 3-phase ACPI prototype is utilized for proof of concept.**

Keywords—soft-switching; auxiliary commutated pole inverter; fixed-timing; variable-timing; frequency response; EMI

I. Introduction

High dv/dt and di/dt rates are a source of high-frequency electromagnetic interference (EMI) [1]. These are inherent to PWM voltage source inverters (VSI) due to their fast-switching semiconductor devices. The poor EMI performance of VSIs impedes their larger integration in electromagnetically sensitive environments such as the More Electric Aircraft (MEA). Furthermore, common mode (CM) EMI in VSI-based motor drives can disrupt the controlled motor [1]. Low power-density passive filters often constitute a post-design solution not entirely suitable for the space- and weight-constrained MEA.

It is therefore preferable that EMI is addressed at source. Switching speeds with optimized slew rates exhibit reduced high-frequency content, which contributes to increased filter power densities [2]. Soft-switching topologies are usually used for switching loss reduction [3]. Most topologies achieve soft switching with a resonant circuit that slows and smoothens the switching magnitude edges. Thus, their slew rates and transitions are not as sharp as in hard-switched VSIs. This is expected to enhance EMI performance.

This paper investigates the auxiliary commutated pole inverter (ACPI). The two common ACPI control schemes, fixed- and variable-timing are examined with regards to output voltage dv/dt control, for predicting and attenuating its high-frequency content. Frequency response analysis and expressions for the ACPI's resonant operation are presented. The implementation of the two ACPI control schemes and their effect on resonance are also discussed.

II. The Auxiliary Commutated Pole Inverter

The ACPI is a modular, highly efficient, PWM-controlled, zero-voltage switching (ZVS) topology [3,4]. As seen in Fig. 1a, a resonant inductor L_r and four auxiliary devices comprise a branch between the output and the dc-midpoint O. L_r and snubber capacitors C_{r1} and C_{r4} form the resonant circuit. Diodes D_{s1} and D_{s4} protect the auxiliary branch in case the inductor current i_{Lr} is interrupted before diminishing to zero. The 3-phase version simply consists of three such circuits, with all the auxiliary branches sharing the dc-midpoint.

Fig. 1b shows i_{Lr} and the output voltage, v_{pole}, during a switching cycle. Before a transition between the main devices (S_1 and S_4), an auxiliary switch (S_{a1} or S_{a4}) turns on and L_r starts accumulating energy during t_{ramp}. Then during t_{res}, resonance occurs between L_r and C_r shaping the v_{pole} edges sinusoidally and optimizing dv/dt compared to a hard-switched inverter. Resonance ends when v_{pole} swings to the opposite rail and is clamped by the corresponding anti-parallel diode.

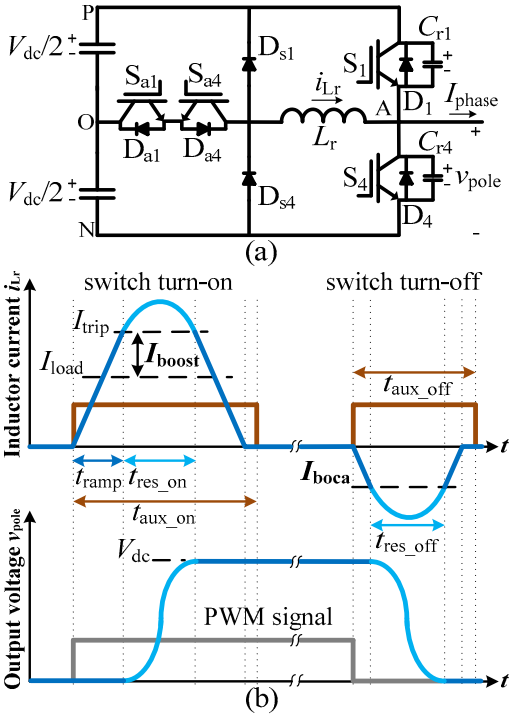

Fig. 1. The auxiliary commutated pole inverter phase-leg (a), ACPI resonant magnitudes during a switching cycle (b).

III. Fourier Series of Sinusoidal Pulses

By successive differentiations in time, a pulse's exponential Fourier coefficients are derived [5]. Equations (1) and (2) describe these coefficients for a trapezoidal and a sinusoidal pulse-train respectively, at a frequency of harmonic number n [5]. For (2), the sinusoidal edges are treated as S-shaped ones because they can be finitely differentiated.

$$c_n = A\frac{\tau}{T_s}\operatorname{sinc}\left(n\omega_s\frac{\tau}{2}\right)\operatorname{sinc}\left(n\omega_s\frac{t_r}{2}\right)e^{jn\omega_s\frac{\tau+t_r}{2}} \quad (1)$$

$$c_n = A\frac{\tau}{T_s}\operatorname{sinc}\left(n\omega_s\frac{\tau}{2}\right)\operatorname{sinc}\left(n\omega_s\frac{t_r-t_{r(dv/dt)}}{2}\right)\operatorname{sinc}\left(n\omega_s\frac{t_{r(dv/dt)}}{2}\right)e^{jn\omega_s\frac{\tau+t_r}{2}} \quad (2)$$

where $\operatorname{sinc}(x) = \sin(x)/x$, A is the amplitude of the pulses, T_s is the period, $\omega_s = 2\pi/T_s$ is the angular frequency, τ is the pulse-width, t_r is the rise/fall time, and $t_{r(dv/dt)}$ is the first derivative rise time found only in (2). Fig. 2 illustrates the pulses in question in the time-domain. They are considered symmetrical, of equal rise/fall times. Ideally, the ACPI produces a sinusoidal v_{pole} pulse-train.

The number of sinc(x) terms in (1) and (2) signifies the number of corner frequencies on each pulse's spectral envelope. Hence, a trapezoidal pulse envelope has two corner frequencies: f_{c1} marks an envelope slope change from 0 to -20 dB/dec, and f_{c2} a change from -20 to -40 dB/dec, as given by (3) and (4), respectively. Therefore, τ mainly influences the lower end of the spectrum, and t_r the higher end [5].

$$f_{c1} = 1/\pi\tau \quad (3)$$

$$f_{c2} = 1/\pi t_r \quad (4)$$

The S-shaped pulse envelope has three frequencies: f_{c1} is given by (3), but now $t_{r(dv/dt)}$ influences f_{c2} and defines f_{c3}, as in equations (5) and (6).

$$f_{c2} = 1/\pi\left(t_r - t_{r(dv/dt)}\right) \quad (5)$$

$$f_{c3} = 1/\pi t_{r(dv/dt)} \quad (6)$$

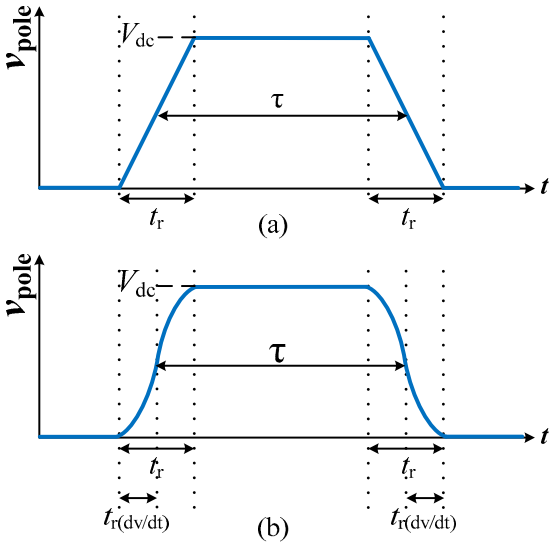

Fig. 2. A trapezoidal pulse (a) and a pulse with sinusoidal edges (b).

The introduction of f_{c3} improves high-frequency attenuation, as it marks an envelope slope change from -40 to -60 dB/dec. A sinusoidal edge can be approximated through the S-shaped one by defining $t_{r(dv/dt)} = t_r/2$. This way, f_{c2} and f_{c3} merge, and the sinusoidal envelope changes directly from -20 to -60 dB/dec. Fig. 3 shows these results for two symmetrical pulses with 50% duty cycle and equal t_r times.

The important attribute of S-shaped/sinusoidal edges is that, unlike the trapezoidal pulse, both their duration (t_r) and shape ($t_{r(dv/dt)}$), i.e., their smooth corners, can be calibrated for predetermining and further attenuating their high-frequency harmonic content. It is then possible for the ACPI to outperform an equivalent hard-switched inverter with regards to high-frequency CM EMI, by actively controlling the edge duration and shape of its output voltage.

IV. Fixed-Timing and Variable-Timing Control

Resonance can be described by a series LC circuit driven by half the dc-link voltage $V_{dc}/2$ and the phase current I_{phase}. Fig. 4 shows the equivalent resonant circuit for a turn-on transition of switch S_1 when $I_{phase} > 0$ along with the appropriate initial conditions. Its solution gives sinusoidal i_{Lr} and v_{pole} expressions:

$$i_{Lr} = I_{phase} + I_{boost}\cos(\omega_0 t) + \frac{V_{dc}}{2Z_0}\sin(\omega_0 t) \quad (7)$$

$$v_{pole} = \frac{V_{dc}}{2}[1 - \cos(\omega_0 t)] + Z_0 I_{boost}\sin(\omega_0 t) \quad (8)$$

Z_0 and ω_0 are the resonant impedance and frequency:

$$Z_0 = \sqrt{L_r/2C_r} \quad (9)$$

$$\omega_0 = 1/\sqrt{2L_rC_r} \quad (10)$$

Substituting the i_{Lr} or v_{pole} value at the end of resonance into (7) or (8), the resonant time t_{res_on} is derived, as is the case for t_{res_off} when the equivalent LC circuit of a given switch turn-off transition is solved. These intervals are the actual v_{pole} rise/fall

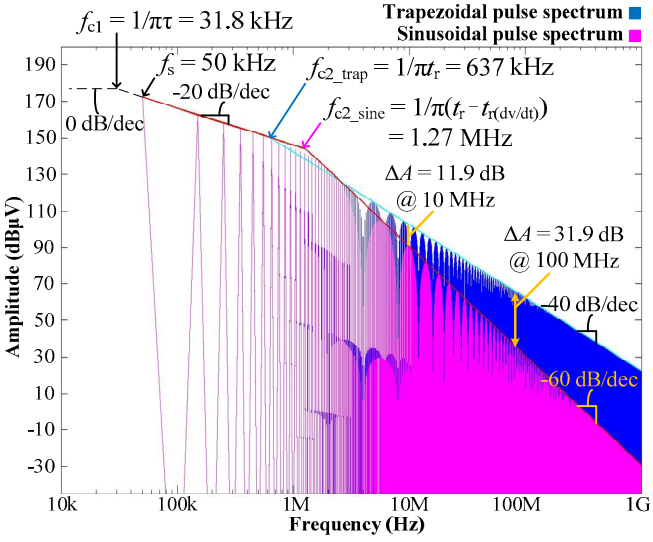

Fig. 3. Trapezoidal and sinusoidal pulse spectra with 50% duty, $V_{dc} = 650$ V, $f_s = 50$ kHz, $\tau = 10$ µs, $t_r = 500$ ns, and $t_{r(dv/dt)} = 250$ ns.

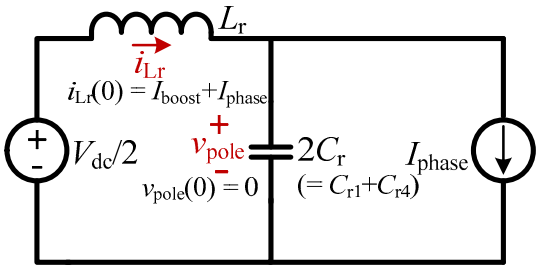

Fig. 4. Equivalent LC circuit of a switch turn-on transition when $I_{phase} > 0$.

times. By controlling t_{res_on} and t_{res_off}, and how resonance occurs overall through the resonant parameters, v_{pole} can assume the desired edges for predetermining its frequency spectrum. Equations (11) and (12) describe t_{res_on} and t_{res_off}:

$$t_{res\_on} = \frac{2}{\omega_0}\tan^{-1}\left(\frac{V_{dc}/2}{Z_0 I_{boost}}\right) \quad (11)$$

$$t_{res\_off} = \frac{2}{\omega_0}\tan^{-1}\left[\frac{V_{dc}/2}{Z_0(|I_{boca}| + I_{phase})}\right] = \frac{2}{\omega_0}\tan^{-1}\left(\frac{V_{dc}/2}{Z_0 I_{off}}\right) \quad (12)$$

For given L_r and C_r values, intervals t_{res_on} and t_{res_off} can be thoroughly controlled through boost currents I_{boost} and I_{boca}, as seen in Fig. 1. This way, during a fundamental cycle T_1, the properties of the resonant intervals can be defined.

In other words, resonance can be controlled in two ways: fixed-timing and variable-timing control. Usually, these terms refer to the gate signal width of the auxiliary switches t_{aux}, (see Fig. 1b) which can be fixed or variable during T_1 [6]. Further, [6] compares the two schemes in terms of applicability and efficiency. Fixed-timing is easier to implement since no current sensing is required to keep t_{aux} fixed but leads to higher auxiliary circuit losses and current stress. Conversely, variable-timing requires more resources to vary t_{aux} according to the I_{phase} level, but exhibits less auxiliary circuit losses and current stress.

In reality, whether t_{aux} is fixed or variable during T_1 is not related to the control being fixed- or variable-timing. However, this terminology is used here to still reflect on the complexity and efficiency of each scheme, with these qualities now depending on the nature of resonance itself, specifically on the boost currents.

In this work, fixed-timing builds i_{Lr} up to the same I_{trip} value for switch turn-ons and the same I_{boca} value for switch turn-offs before resonance starts, throughout T_1. Hence, the t_{ramp} intervals of both kinds of transition are kept fixed, which further means that I_{boost} varies and I_{boca} is fixed (meaning that $I_{off} = I_{boca} + I_{phase}$ varies) during T_1. Hence, from (11) and (12) the t_{res} intervals vary from one switching cycle to the next. On the other hand, variable-timing control requires I_{phase} sensing in order to build i_{Lr} up to the appropriate I_{trip} and I_{boca} values in a given switching cycle. This way t_{ramp} varies throughout T_1 which means that I_{boost} is fixed and I_{boca} varies (in a way that I_{off} remains fixed). Consequently, (11) and (12) result in fixed t_{res} intervals from one switching cycle to the next.

t_{aux} is kept fixed regardless of the control scheme. It just has to be large enough for the auxiliary circuit to go through its full operational cycle during a transition. Essentially, the terms fixed- and variable-timing now refer to the nature of the t_{ramp} interval, a crucial control parameter.

Proper boost current selection is the fundamental aspect in actively controlling the properties of the ACPI resonant magnitudes [7]. Specifically, the magnitude and pulse-width of i_{Lr} determine the losses in the auxiliary branch and overall current stress, and more importantly, the v_{pole} edge properties influence the EMI performance of the inverter.

Fixed-timing control results in t_{res} intervals, i.e., in v_{pole} rise/fall times that are unequal in duration throughout T_1 and inconsistent in shape. Thus, the frequency response of v_{pole} cannot be easily predicted, since the initial conditions of the equivalent LC circuit are different every time. This means that each and every resonance during the ACPI's fundamental cycle is driven with varying amounts of energy. In contrast, variable-timing control results in fixed t_{res} intervals and thus v_{pole} edges that are the same throughout T_1, since the amount of energy put into resonance is consistent. The v_{pole} pulse-train is then simplified with respect to its edges. Thus, its frequency response is made more predictable, on par with the pulses of Fig. 3, even though v_{pole} is now Sinusoidal- or Space Vector-modulated (SPWM or SVPWM). For this reason, this work omits using just the snubber capacitors for realising switch turn-offs at high I_{phase} levels [4,6] (thus bypassing the auxiliary circuit and producing linear edges), as to keep the edges of the v_{pole} pulse-train purely sinusoidal. Fig. 5 shows v_{pole} for two switching cycles under fixed- and variable-timing control.

Fig. 6 shows the i_{Lr} pulses between the two control schemes during a fundamental quarter-cycle $T_1/4$ (consisting of only four switching cycles for simplicity). With fixed-timing, the pulses reach the same I_{trip} and I_{boca} levels before resonance, regardless of the I_{phase} level. The more complex variable-timing scheme however, builds i_{Lr} up to a value depending on the I_{phase} level. Clearly, variable-timing control leads to less auxiliary circuit loss and overall current stress.

V. Implementation of the Two Control Schemes

Fixed-timing control requires the direction of I_{phase} for selecting the appropriate auxiliary switch for a given transition. S_{a1} assists in switch turn-ons and S_{a4} in switch turn-offs when $I_{phase} > 0$. The reverse applies when $I_{phase} < 0$. Normally, I_{trip} and I_{boca} should be large enough to overcome the damping effect of the auxiliary circuit's parasitic resistance and allow full resonance. This means that v_{pole} should completely swing from one rail to the other for successful ZVS. This control can be simplified greatly if $I_{trip} = I_{boca}$ meaning that at the control level the t_{ramp} intervals are made equal for both kinds of transition. Consequently, no I_{phase} information is needed with less computational effort. Simply, the t_{ramp} intervals are manually input to the control algorithm. The disadvantage is that, since full resonance must be realised at all times, the i_{Lr} pulses will become unnecessarily large, regardless of I_{phase} level, adverse to the ACPI's current stress and efficiency. Regardless, this approach was taken for simplifying control since at this stage efficiency is not the primary concern.

Variable-timing control requires knowledge of both the magnitude and the direction of I_{phase}, as well as the magnitude of V_{dc} to generate the PWM signals, as seen by expressions (13) and (14):

$$t_{ramp\_on} = \frac{L_r I_{trip}}{V_{dc}/2} = \frac{L_r(I_{boost} + I_{phase})}{V_{dc}/2} \quad (13)$$

$$t_{ramp\_off} = \frac{L_r I_{boca}}{V_{dc}/2} = \frac{L_r(I_{off} - I_{phase})}{V_{dc}/2} \quad (14)$$

Since V_{dc} is fixed, the t_{ramp} intervals, and by extension I_{trip} and I_{boca} depend on the level of I_{phase} during the given switching cycle. This scheme forces I_{boost} and the sum $I_{off} = I_{boca} + I_{phase}$ to be fixed during T_1, per (11) and (12). This way, t_{res_on} and t_{res_off} remain fixed and the edges of the v_{pole} pulse-train are consistent in duration and shape as seen in Fig. 5b. Symmetry in the pulses can be achieved by further demanding that $I_{boost} = I_{off}$, resulting in $t_{res\_on} = t_{res\_off}$. This is desirable because the frequency response of a symmetrical pulse-train is simpler [8] and thus more predictable. The disadvantage is that the boost current condition $I_{boost} = I_{off} \geq I_{phase\_pk}$ should apply (where I_{phase_pk} is the peak phase current), if resonance is to transpire throughout T_1 and the v_{pole} edges are shaped sinusoidally. The consequence is once again

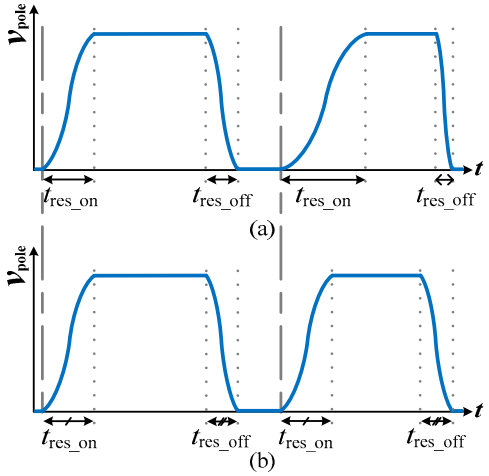

Fig. 5. Part of the v_{pole} pulse-train under fixed-timing (a), and under variable-timing control (b) when $I_{phase} > 0$.

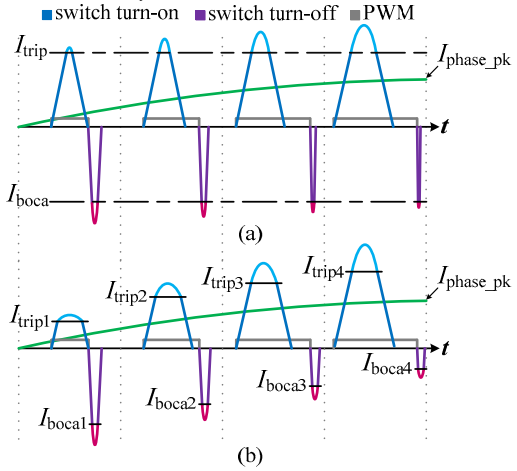

Fig. 6. Comparison of i_{Lr} pulses with fixed-timing (a), and variable-timing control (b) during a fundamental quarter-cycle.

higher auxiliary circuit loss and current stress, but not as high as an equivalent fixed-timing scheme would cause.

Soft-switching is successful not only when v_{pole} swings to the opposite rail but also when i_{Lr} diminishes to zero. But this is not guaranteed if the PWM signal assumes short pulse-widths, due to increases in the switching frequency f_s or the modulation index m_A. Assuming the i_{Lr} pulses are large enough for successful ZVS operation, a limit on their width has to be imposed. Thus, the first control parameter is set, the t_{aux} interval that should accommodate the maximum i_{Lr} pulse-width that appears during T_1. That should happen during the switch turn-on transition at I_{phase_pk}, regardless of the control scheme. As mentioned, t_{aux} is kept fixed, and is now assigned the value of $d_{min}T_s$, where d_{min} is the minimum duty cycle imposed by the modulation scheme and T_s is the switching period.

Once t_{aux} is set, a variable-timing scheme is designed based on the desirable t_{res} intervals. These are selected for an optimized v_{pole} frequency response with regards to that of an equivalent hard-switched inverter, by exhibiting a corner frequency f_{c2} early in the spectrum and also a -60 dB/dec high-frequency attenuation. Then, since t_{ramp} varies throughout T_1, a maximum value is selected for never violating the condition $t_{aux} = t_{res} + 2t_{ramp\_max}$. Also, v_{pole} should ideally be symmetrical. Thus, the minimum boost current condition $I_{boost} = I_{off} = I_{load\_pk}$ should apply, to always guarantee resonance. This further means that at I_{phase_pk}, $I_{trip\_max} = 2\,I_{phase\_pk}$. Hence, (13) becomes:

$$L_r = \frac{V_{dc} t_{ramp\_max}}{4 I_{phase\_pk}} \quad (15)$$

Then, (11) along with (9) and (10) are used for calculating C_r. After designing the variable-timing scheme, a fixed-timing scheme was chosen with the condition that the resulting maximum t_{res} interval was equal to the variable-timing ones. The current stress of this fixed-timing scheme was then estimated for sizing the semiconductor devices of the topology.

VI. Experimental Results

Fig. 7 shows the 3-phase ACPI prototype. A resonant inductor of 2.7 μH and two snubber capacitors of 47 nF complement each phase. $t_{ramp\_on} = t_{ramp\_off} = 400$ ns is input to the fixed-timing algorithm, ideally giving $I_{trip} = I_{boca} = 36$ A and a maximum t_{res} of 1.2 μs. Conversely, variable-timing is realized through the online calculation of (13) and (14) by sensing the dc-link voltage and the three phase currents, while also inputting $I_{boost} = I_{off} = 18$ A ($= I_{phase\_pk}$) to ideally achieve $t_{res\_on} = t_{res\_off} = 1.2$ μs throughout T_1. The direction of I_{phase} is used to select the appropriate auxiliary switch for a given transition in that phase. No v_{pole} sensing is needed. Instead, a fixed 1.2-μs delay is introduced for gating on the incoming device from when resonance is initiated.

A 5-kW EA-PS8500-30 power supply supplies the dc-link. The modulation scheme is SPWM with $f_1 = 400$ Hz fundamental frequency, $f_s = 20$ kHz, and $m_A = 0.83$. The symmetrical, star-connected load is $R = 10\ \Omega$ and $L = 2$ mH per phase. Experimental results are presented for phase A only.

With 3-phase symmetry, the resonant actions occur similarly in all phases.

Fig. 8 shows the phase A current i_A and its inductor current i_{LrA} over two fundamental cycles, under the two soft-switching schemes. Fixed-timing control leads to unnecessarily high i_{LrA} pulses throughout T_1. This is not the case for variable-timing control. The amounts of energy used during each resonant transition throughout T_1 are according to the phase current level, with an impact on the inductor current. As a result, the inductor rms current is 10.2 A with variable-timing, 2 A smaller than with fixed-timing. The phase current is 12 A rms.

Fig. 9 compares the transitions of S_1 near I_{A_pk} under hard-switching and the two soft-switching schemes. The turn-off transition is followed by the turn-on one. The hard-switched transitions occur quickly, and the v_{pole} edges are linear in shape. Soft-switching results in smoother edges that are up to six times slower. The dv/dt is then optimized, ideally having a sinusoidal trend due to resonance. However, secondary effects like parasitic inductance in the output node, contribute to a non-ideal edge shape. Also, ringing at 1.6-MHz is observed between the parasitic inductance of the switching loop and the snubber capacitors. Hard-switching does not exhibit this. Fixed-timing control leads to v_{pole} edges of unequal duration by almost 400 ns. Moreover, the two i_{LrA} pulses are close in height, even if the turn-off pulse need not be that large. In contrast, variable-timing control generates v_{pole} edges of almost equal duration. The i_{LrA} pulses are also more related to the phase current level, with the turn-off pulse being 26.6 A smaller than the turn-on one. Variable-timing seems to offer better results in these key areas than fixed-timing.

Fig. 10 compares hard-switching and the two soft-switching schemes with regards to the v_{pole} frequency spectrum. Twenty fundamental cycles of the time-domain waveforms are taken at V_{dc} = 450 V with a Rohde & Schwarz RTO1024 oscilloscope. A resolution of 5 ns and a sample rate of 200 MSa/s give a record length of 10 MSa for each waveform. The noise floor at high frequencies is decreased by averaging the waveforms 5000 times. Then, Matlab performs an optimized Fast Fourier Transform algorithm on the time-domain data to obtain the frequency-domain results. Soft-switching reduces the high-frequency content of the v_{pole} pulse-train with regards to hard-switching. Whilst the PWM region of the spectrum is similar for all three schemes, in the hundreds of kHz range, soft-switching exhibits better attenuation, because of the longer and smoother edges. Thus, the -40 dB/dec region appears earlier than hard-switching, and most importantly, the -60 dB/dec slope appears which contributes even more in high-frequency attenuation. Variable-timing has the best performance, since it generates long, smooth edges of around 1.2 µs throughout T_1, and the f_{c3} corner frequency appears earlier than the fixed-timing one. Both soft-switching schemes result in a maximum attenuation of 33 dBµV at 4.5 MHz.

The spectral envelopes and the corner frequencies are approximated in Fig. 10, as well. The hard-switched pulses are asymmetrical, with edges of around 650 ns when i_A is low,

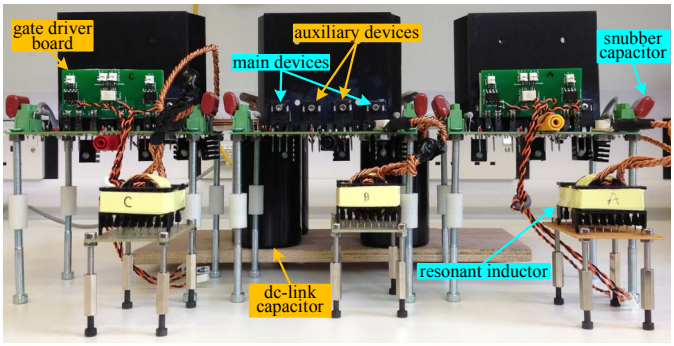

Fig. 7. The 3-phase ACPI prototype.

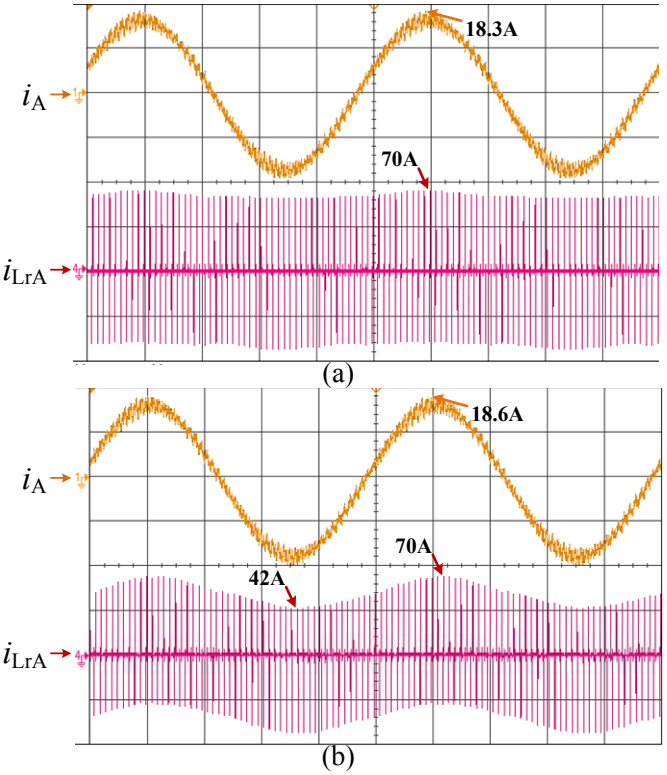

Fig. 8. Phase A current i_A and inductor current i_{LrA} under fixed-timing (a), and variable-timing control (b). i_A 10 A/div, i_{LrA} 40 A/div, timescale 0.5 ms/div.

resulting in an intermediate slope and two f_{c2} corner frequencies as given by (4) between the -20 and -40 dB/dec regions [8]. They agree well with the duration of the edges. The low-frequency slope of the soft-switching spectra is not exactly -20 dB/dec, and as such no f_{c2} frequencies as given by (5) can be confidently approximated. The regions of -40 and -60 dB/dec suggest the existence of f_{c3} corner frequencies as given by (6). The f_{c3} of the fixed-timing envelope suggests $t_{r(dv/dt)}$ = 290 ns, and the variable-timing one suggests $t_{r(dv/dt)}$ = 530 ns. Variable-timing appears to produce smoother edges, and to do so more consistently as the v_{pole} pulse-train is more symmetrical than with fixed-timing. In practice however, it is difficult to discern any corners due to the 1.6-MHz ringing, and other high-frequency phenomena as seen in Fig. 9, such as the voltage drop attributed to parasitic inductance right before the edges materialize. Furthermore, both soft-switching schemes seem to produce more S-shaped than sinusoidal edges, as attested by the -40 dB/dec slope.

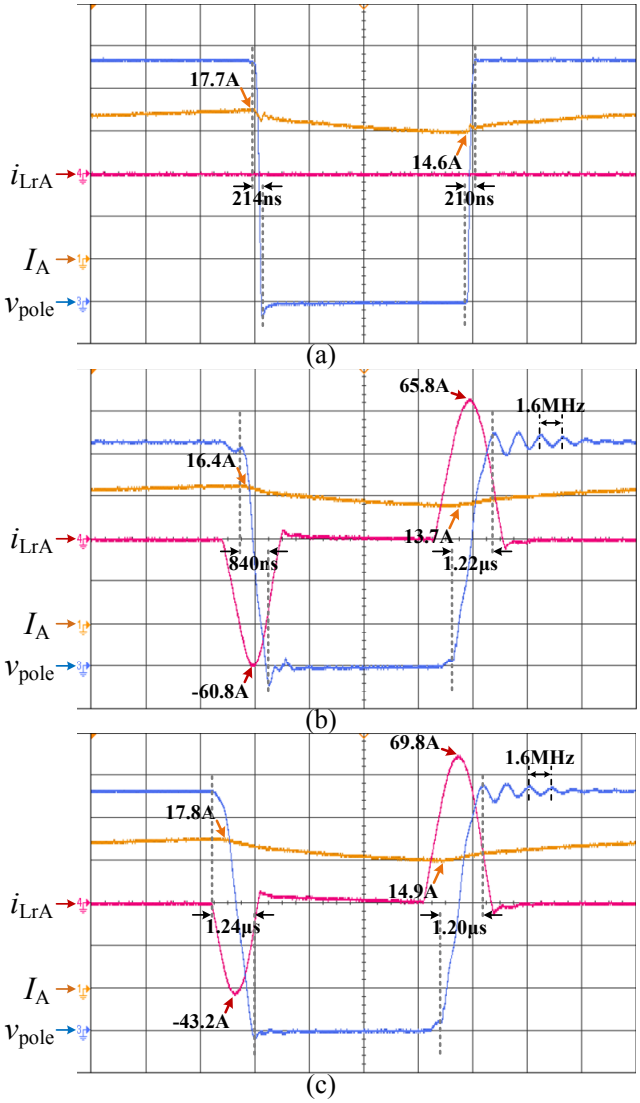

Fig. 9. Transitions under hard-switching (a), fixed-timing (b), and variable-timing control (c) near I_{A_pk}. I_A 5 A/div, v_{pole} 80 V/div, i_{LrA} 20 A/div, timescale 1.6 µs/div.

The frequency of any time-domain ringing, appears with exacerbated content in the spectrum [9]. Hence, increased content appears around 1.6 MHz in the soft-switching spectra. The other high-frequency phenomena observed in Fig. 9 are also present, and are manifested up to 4 MHz. Beyond that point, the noise floor is reached. These phenomena interrupt the -60 dB/dec region and increase the high-frequency content. The hard-switching spectrum has more high-frequency content, and as such, it reaches the noise floor later, at around 25 MHz.

VII. Conclusions

The auxiliary commutated pole inverter (ACPI) shapes the edges of its output voltage (v_{pole}) by controlling the resonant circuit parameters. Thus, its frequency response can be predicted as a step towards enhancing the CM EMI performance of VSIs. Two control schemes, fixed- and variable-timing control, are presented through the perspective of the resonant circuit

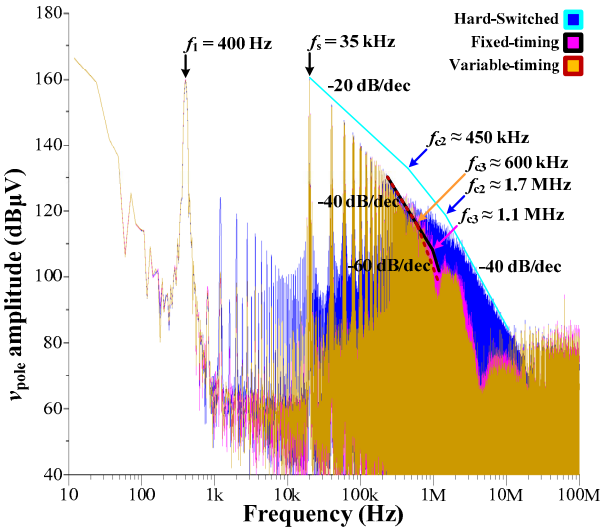

Fig. 10. Experimental v_{pole} frequency spectrum under the hard-switched (blue), fixed-timing (magenta), and variable-timing (orange) schemes.

properties, specifically the boost currents. Fixed-timing is simpler but leads to large inductor current pulses and an asymmetrical v_{pole} pulse-train. Variable-timing is more complex but can reduce current stress and increase efficiency, whilst giving a more predictable v_{pole} frequency response. A 3-phase, 5-kW ACPI prototype was used for proof of concept. Both control schemes produce longer and smoother v_{pole} edges than hard-switching, which introduces a -60 dB/dec spectral envelope and improves high-frequency attenuation. Variable-timing has the best performance as it generates a symmetrical v_{pole} pulse-train of long, smooth edges of 1.2 µs.

References

[1] M. Cacciato, A. Consoli, G. Scarcella, and A. Testa, "Reduction of common-mode currents in PWM inverter motor drives," *IEEE Trans. Ind. Appl.*, vol. 35, no. 2, pp. 469-476, Mar.-Apr. 1999.

[2] J. Shao, R. L. Lin, F. C. Lee, and D. Y. Chen, "Characterization of EMI performance for hard and soft-switched inverters," *IEEE Appl. Power Electron. Conf. and Exp. (APEC 2000)*, 2000, vol. 2, pp. 1009-1014.

[3] V. Pickert and C. M. Johnson, "Three-phase soft-switching voltage source converters for motor drives. I. Overview and analysis," *IEE Proc. on Electric Power Appl.*, vol. 146, no. 2, pp. 147-154, Mar. 1999.

[4] R. W. De Doncker and J. P. Lyons, "The auxiliary resonant commutated pole converter," *IEEE Ind. Appl. Soc. Annu. Meeting*, 1990, vol. 2, pp. 1228-1235.

[5] N. Oswald, B. H. Stark, D. Holliday, C. Hargis, and B. Drury, "Analysis of shaped pulse transitions in power electronic switching waveforms for reduced EMI generation," *IEEE Trans. Ind. Appl.*, vol. 47, no. 5, pp. 2154-2165, Sept.-Oct. 2011.

[6] K. Ma, D. Xu, T. Zhang, and S. Igarashi, "The evaluation of control strategies for auxiliary resonant commutated pole inverter," *IEEE Energy Conv. Congr. and Expo. (ECCE 2009)*, 2009, pp. 810-816.

[7] A. Charalambous, X. Yuan, N. McNeill, Q. Yan, and N. Oswald, "EMI reduction with a soft-switched auxiliary commutated pole inverter," *IEEE Energy Conv. Congr. and Expo. (ECCE 2015)*, 2015, pp. 2650-2657.

[8] A. Nagel and R. W. De Doncker, "Analytical approximations of interference spectra generated by power converters," *IEEE Ind. Appl. Conf. (IAS '97)*, 1997, vol. 2, pp. 1564-1570.

[9] C. R. Paul, *Introduction to Electromagnetic Compatibility*, 2nd ed. Hoboken, NJ: Wiley, 2006.